

PAPER • OPEN ACCESS

Numerical methodology to predict and analyze cavitating flows in a Kaplan turbine

To cite this article: Flavia Turi and Regiane Fortes-Patella 2019 *IOP Conf. Ser.: Earth Environ. Sci.* **240** 022019

View the [article online](#) for updates and enhancements.

Numerical methodology to predict and analyze cavitating flows in a Kaplan turbine

Flavia Turi, Regiane Fortes-Patella

Univ. Grenoble Alpes, Grenoble INP, CNRS, LEGI F-38000 Grenoble, France

E-mail: flavia.turi@legi.grenoble-inp.fr, regiane.fortes@legi.grenoble-inp.fr

Abstract. A computational methodology to predict the appearance and the evolution of the cavitation phenomena in a scale model of a 5-blades Kaplan turbine was developed. The cavitating flow was modeled by a homogeneous approach with a barotropic state law and the $k - \omega$ SST turbulence model. *RANS* simulations were performed, near the *Best Efficiency Point*, on two computational domains (**D1** and **D2**) comprising one periodic interblades channel consisting of the guide vanes, the runner blade and the cone (domain **D1**) or taking into account the entire draft tube (domain **D2**). At first, non-cavitating simulations were carried out in domain **D1** in order to match numerical conditions to the experimental ones (similar mass flow Q , head H and mainly the torque T) via an iterative procedure. From this reference operating point obtained in free-cavitation regime, cavitating simulations were performed on both computational domains by reducing the *Thoma number*, σ . Two different inlet boundary conditions were tested: the classical one, imposing the mass flow rate Q ; the new one, fixing the total pressure and, consequently, keeping the machine head H constant during the cavitation drop, as in experiments. In all the performed calculations, the outlet boundary condition is given by a constant static pressure. Computed torque and efficiency drop curves were compared to available experimental data. The best results were obtained with the computational domain **D2** applying a constant total pressure on the inlet. The torque and efficiency evolutions were well-predicted with the proposed calculation methodology, and the numerical cavitation structures agreed with experimental observations. Analyses of the blade loading during cavitation breakdown are also proposed in the article. Unsteady simulations are under investigation to improve the prediction and the analyses of more developed cavitating regimes.

1. Introduction

Nowadays, the continue diminution of the non-renewable fossil energy and the exigency to reduce the greenhouse gas emission has boosted the development of hydraulic machines, as Kaplan turbines. The peculiarity of these machines is the flexibility: the guide vane opening and the runner blade position can be continuously regulated during machine operation to maximize the efficiency for a large range of operating conditions. However, this implies the presence of shroud and hub gaps that leads to cavitation phenomena in the runner. Vapor structures can cause several structural damages and changes on the turbine efficiency. For these reasons, the development of a numerical procedure able to characterize the cavitation phenomena inside the turbines and predict their impact on the machine performances is of great industrial interest. Numerical studies of cavitating flows in hydraulic machineries have been usually performed making use of a homogeneous flow approach coupled with cavitating models for the liquid/vapor mixture, such as the barotropic law [1] or Rayleigh-Plesset based models, as the Shingal [2] and the Zwart [3] models. In the case of Kaplan turbines, studies using Rayleigh-



Plesset based models have been proposed by Balint *et al.* [4] and Leguizamón *et al.* [5]. *RANS* equations have been solved on reduced computational domains, including a single interblades channel of the distributor and the runner. A similar approach has been used to simulate a complete machine in steady and transient conditions by Jošt *et al.* [6]. Those simulations have been performed fixing the inlet mass flow rate and have resulted in some mismatches between numerical predictions and experimental observations. Indeed, during the laboratory tests, the machine head is usually imposed as constant in the cavitation breakdown investigations. On the contrary, in the simulations, the machine head cannot be controlled if the inlet discharge is imposed.

In this context, the aim of the present investigation is to develop a numerical methodology able to improve the prediction of the evolution of cavitating flow inside a Kaplan turbine. The analysis refers to a scale model of a Kaplan turbine consisting of five blades, tested in the *GE Renewable Energy* laboratory in Grenoble (France). The three-dimensional *RANS* equations have been solved with the commercial code FINETM/Turbo, which applies a homogeneous approach and a barotropic state law developed in the laboratory *LEGI* to model the cavitating flow [1]. Preliminary simulations have been run on a full-periodic single interblades channel comprising the guide vane, the runner and the cone. At first, the machine operating point has been fixed in non-cavitating regime, iteratively varying the inlet mass flow rate to target the experimental torque value. Subsequently, cavitation calculations have been performed with the founded mass flow rate as inlet boundary condition. Afterwards, the numerical domain has been extended including the draft tube in order to consider in the analysis its influence on the flow and, consequently, on the numerical cavitation predictions. At last, the total pressure has been imposed on the inlet instead of the mass flow rate, fixing the machine head. This has allowed to perform calculations as the experiments.

The article is structured as follows: the section 2 describes the theoretical models applied to simulate cavitation and turbulence phenomena inside of the turbine. The tested calculation methodologies are discussed in section 3. Simulations have been performed on two computational domains and different inlet boundary conditions have been tested. The main global and local numerical results are presented in section 4, where comparative studies with experiments are also proposed to validate the numerical approaches and to select the best methodology. Finally, the investigation conclusions are presented.

2. Theoretical models

The modeling of a two-phase flow inside a turbomachinery is complex and presents very high computational cost. An alternative approach, proposed by Ishii *et al.* [7], consists to consider the cavitating flow as a homogeneous mixture of liquid and vapor. The homogeneous approach relays on the hypothesis that the mixture density ρ changes in the flow field between the vapor density ρ_V and the liquid density ρ_L as a function of the equivalent void ratio α of the liquid-vapor mixture according to equation 1

$$\rho = \alpha \rho_V + (1 - \alpha) \rho_L . \quad (1)$$

Assuming that the pure phases in the mixture are incompressible and share the same instantaneous velocity, pressure and turbulence fields, only one set of *RANS* equations can be used to describe the flow motion. However, a model for the cavitating flow and for the averaged Reynold's stress terms is required to close the governing equations.

2.1. Cavitation model

The cavitation model used in this work is the barotropic law. This approach has been initially proposed by Delannoy and Kueny [1] and was largely used to predict cavitation phenomena in

pumps, e.g. see Refs. [8, 9, 10]. In this formulation, the evolution of the mixture density ρ and the local static pressure P are strongly linked via a barotropic state law $\rho = \rho(P)$, shown in figure 1.

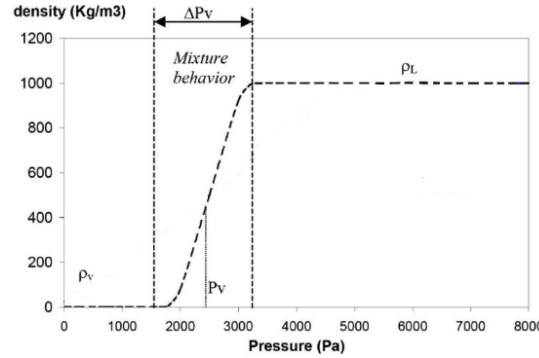


Figure 1. Barotropic law $\rho = \rho(P)$.

When the pressure is higher or lower than the vapor pressure P_V , the fluid is supposed to be purely liquid or purely vapor. In the mixture region, $P_V - \Delta P < P < P_V + \Delta P$, where ρ rapidly varies between the liquid density ρ_L and the vapor density ρ_V , a sinusoidal function is used to describe the mixture density, defined as:

$$\rho = \frac{\rho_L + \rho_V}{2} + \frac{\rho_L - \rho_V}{2} \sin\left(\frac{P - P_V}{A_{min}^2}\right). \quad (2)$$

In the equation 2, the parameter A_{min} represents the slope of this evolution law defined as:

$$A_{min} = \sqrt{\frac{\rho_L - \rho_V}{2}} c_{min}^2, \quad (3)$$

with c_{min} indicating the minimal value of the sound velocity in the liquid–vapor mixture. Following previous studies [11, 12], c_{min} is assumed to be equal to 1 m/s, the density ratio between the vapor and the liquid phase is set to 0.01 and the coefficient A_{min} is equal to 23.

2.2. Turbulence model

The turbulence model used in this work is the well-known $k - \omega$ SST, presented the first time by Menter *et al.* [13]. This model combines the $k - \omega$ approach in the boundary regions and the $k - \varepsilon$ in the free stream flow. The choice of the turbulence model imposes limitation in the wall mesh sizing. To obtain physical correct results with the $k - \omega$ SST, the dimensionless wall distance y^+ must be less than 10.

3. Numerical methodology

The numerical methodology developed to predict the cavitating flow behavior and its effect on the turbine performance will be now presented. The methodology applies the commercial code FINETM/Turbo and has been validated by experimental data furnished by the *GE Renewable Energy Laboratory* in Grenoble (France). Cavitating (CAV) and non-cavitating (NCAV) calculations are steady and concerns operating conditions (mass flow Q , turbine head H , and torque T) near to the *Best Efficiency Point* (BEP).

3.1. Calculation domains

The investigated machine is a reduced-scale Kaplan turbine developed and tested at the *GE Renewable Energy Laboratory* in Grenoble (France). The turbine has a 24-guide vanes distributor and a 5-blades runner. Two partial computational domains have been considered in the numerical analyses:

- (i) The first domain, **D1**, shown in figure 2 (a), includes a single interblades channel consisting of the guide vane, the runner blade and the cone. Periodic boundary conditions are imposed to simulate the entire machine.
- (ii) The second domain, **D2**, illustrated in figure 2 (b), includes the domain **D1** and the draft tube.

Table 1. Mesh characteristics of the numerical domain **D1**.

Component	Number of elements	Min. skewness	Max. expansion ratio	y_{mean}^+
Guide vane	0.8M	44°	1.7	1
Runner	8.1M	9°	4.5	1.6
Cone	4.7M	15°	1.8	1.1
<i>Total</i>	13.6M			1.2

Table 2. Mesh characteristics of the numerical domain **D2**.

Component	Number of elements	Min. skewness	Max. expansion ratio	y_{mean}^+
Guide vanes	0.8M	44°	1.7	1
Runner	8.1M	9°	4.4	2
Draft tube	5.9M	18°	1.8	8.7
<i>Total</i>	14.8M			8.5

The tip and hub clearances, typical of Kaplan turbines, are considered in all calculations since well description of the flow through these gaps is fundamental to determine the behavior of the hub and the blade tip cavitation regions. Mixing planes separate rotor and stator parts, as indicated in figure 2. To reduce the computational costs, the semi-spiral casing has not been taken into account in the calculation domain. The velocity profiles at the outlet of the spiral casing was evaluated from complementary experimental and numerical studies carried-out previously. Those results have been applied as boundary conditions at the guide vane inlet (see Section 3.2). The numerical domains have been discretized by a fully-structured mesh approach involving only hexahedral cells, achieved using the *Numeca* software *AutoGrid 5*. Mesh optimization studies have been performed on both numerical domains. Starting from very coarse meshes, the elements have been increased until a convergence condition has been reached. The principal characteristics of the resulted meshes are reported in table 1 for **D1** and in table 2 for **D2**. The quality of the discretization has been evaluated by the skewness (i.e. the cells orthogonality) and the expansion ratio (i.e. the ratio between two neighboring cells volumes).

3.2. Inlet and outlet boundary conditions strategies

3.2.1. Non-cavitation conditions To define a numerical methodology able to predict cavitating phenomena in the analyzed system, the first step has been to ensure a correct numerical reproduction of the turbine operating point in non-cavitating conditions. The operating points of a turbine are usually defined by the mass flow, Q , the head, H and the torque, T . Classical boundary conditions have been initially applied on the domain **D1** imposing inlet mass flow and

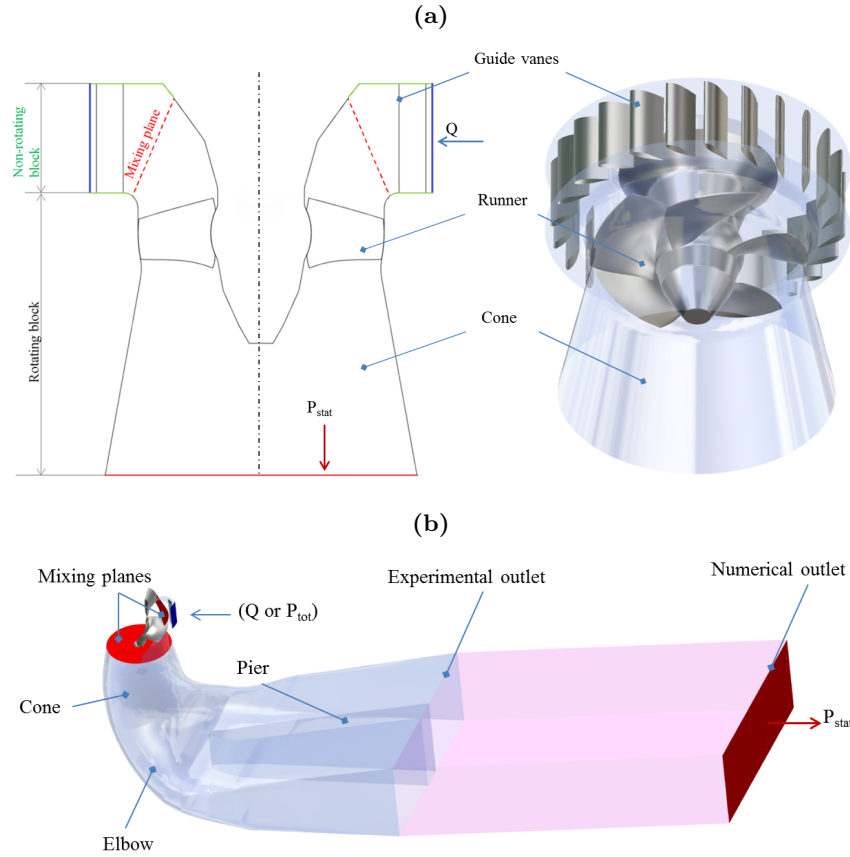


Figure 2. Numerical domains with the used boundary conditions; in both figures, the inlet is in blue and the outlet in red. (a) Domain **D1**, left: meridional view, right: 3D view. (b) Domain **D2**: includes the domain **D1** and the draft tube.

outlet static pressure (figure 2 (a)). Assuming an uniform flow at the distributor inlet section, S_{in} , and at the draft tube outlet section, S_{out} , the experimental value of the turbine head H_{exp} is evaluated by:

$$H_{exp} = \frac{(P_{in} - P_{out})}{\rho g} + \frac{1}{2g} \left(\frac{Q}{\rho} \right)^2 \left(\frac{1}{S_{in}^2} - \frac{1}{S_{out}^2} \right), \quad (4)$$

where P_{in} and P_{out} are the pressures measured at the sections S_{in} and S_{out} , respectively. In the considered numerical domains, the positions of the inlet and the outlet sections differ from the experimental setup so the computed and measured heads cannot be directly compared. To obtain a reliable agreement between experimental and numerical results, preliminary iterative simulations in non-cavitating regime have been performed in domain **D1**, varying the inlet mass flow rate to target the experimental value of the torque. This parameter has been chosen in order to obtain a fluid dynamic agreement with experiments since it is strictly linked to the flow incidence on the runner blade. A reduced difference between experimental and numerical torques ensures the correct reproduction of the work of the turbine.

Applying this procedure, a mismatch between measured and computed torque less than 1% was achieved, with an acceptable discrepancy of the 2.5% between experimental and numerical mass flow rate (see table 3). For clarity reasons, the obtained mass flow rate will be referred as Q_{cor} to distinguish it from the experimental value Q_{exp} .

3.2.2. Cavitation conditions In cavitating regime, two inlet boundary conditions have been tested and compared on domains **D1** and **D2** (as reported in figure 2):

- (i) The Q_{cor} , coupled with computed velocity profiles coming from the stay ring;
- (ii) The total pressure, P_{tot} , calculated from the previous simulation on the domain **D2**. This inlet boundary condition allows to fix the machine head and let the mass flow rate varying with the cavitation development (during cavitation breakdown laboratory tests, the mass flow rate could change of almost 0.5% for the considered operating point).

In all of the performed simulations, a fixed static pressure equal to the ambient pressure is imposed on the outlet, and the cavitation phenomena have been introduced increasing the relative vapor pressure P_V .

4. Analysis of results

4.1. Simulations in non-cavitating regime

Table 3 summarizes numerical global results obtained in non-cavitating conditions on both the computational domain **D1** and **D2**. Firstly, considering the methodology presented in the section 3.2, the inlet mass flow rate has been iteratively tuning on the **D1** in order to achieve $T_{num} \sim T_{exp}$.

Table 3. Comparison between experimental data and results in non-cavitating regime on **D1** and **D2**.

Computational domain	Inlet	$\Delta Q = \frac{(Q_{exp}-Q_{num})}{Q_{exp}}$	$\Delta T = \frac{(T_{exp}-T_{num})}{T_{exp}}$
D1	Q_{exp}	0%	13%
	Q_{cor}	2.5%	< 1%
D2	Q_{cor}	2.5%	< 1.5%

Subsequently, the obtained mass flow value Q_{cor} has been imposed as inlet on the domain **D2**. The presence of the draft tube has produced a reduction of the torque value. Nevertheless, the discrepancy between the computed and measured torque values is less than 1.5%, so still acceptable.

4.2. Simulations in cavitating conditions: global performance analyses

Generally, the evolution of the machine performances with the cavitation development is evaluated by the σ -break curve. This curve represents the machine efficiency η as function of the *Thoma* number, σ , respectively defined as:

$$\eta = \frac{T\omega}{gHQ}, \quad \sigma = \frac{NPSH}{H}. \quad (5)$$

In the σ definition, the *NPSH* represents the net positive suction head. As the head, the experimental evaluation of the *NPSH* depends on the position of the considered domain outlet section:

$$NPSH_{exp} = \frac{(P_{out} - P_V)}{\rho g} + \frac{1}{2g} \left(\frac{Q}{\rho S_{out}} \right)^2, \quad (6)$$

In the case of the simulations performed on the domain **D1**, a direct comparison between numerical and experimental *NPSH* and σ values is not ensured. The machine efficiency η is function of the torque, T , the machine head, H , the mass flow rate, Q , the rotational speed,

ω , and the gravitational acceleration, g . Considering that ω is constant, the σ -break curve can be determined by the evolution of the T , the H and the Q as function of the σ value. Experimentally, a decrease of the torque with the cavitation development (corresponding to the reduction of the σ values) has been observed. Three different computational strategies, presented in table 4, have been tested in order to simulate the torque drop under similar conditions to experiments. The numerical predictions of the torque are compared with experimental data in figure 3(a).

Table 4. Performed calculation strategies.

Strategies	Domain	Inlet BC	Outlet BC	$\Delta H_{max} = \frac{(H_{max} - H_{NCAV})}{H_{NCAV}}$	$\Delta Q_{max} = \frac{(Q_{max} - Q_{NCAV})}{Q_{NCAV}}$
A	D1	Q_{cor}	P_{stat}	1.3%	0%
B	D2	Q_{cor}	P_{stat}	2%	0%
C	D2	P_{tot}	P_{stat}	0.1%	0.5%

(ΔH_{max} and ΔQ_{max} are the maximum difference between computed and measured values)

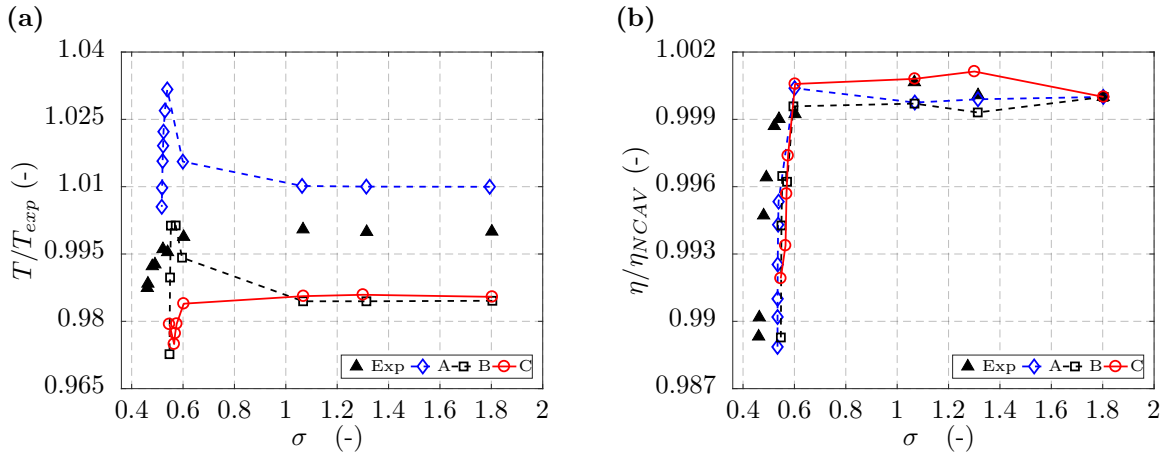


Figure 3. (a) Normalized torque evolution as function of σ and (b) σ -break curve. Experimental measurements are reported with black triangles. Numerical predictions obtained with: **A** strategy are reported with blue diamonds and the dashed line; **B** strategy are indicated with dashed black line and squares; **C** methodology are shown with the red line and the circle symbols.

In simulations performed imposing a constant mass flow rate as inlet boundary condition (**A** and **B**), the head H changes with the increase of the cavitation in the machine, influencing the σ -break curve. Indeed, in these cases, numerical and experimental operating conditions are not really comparable and, as a consequence, the relative computed torque evolution do not agree with experimental results for reduced σ values. At $\sigma = 0.60$ (experimental efficiency drop beginning point) the torque starts to increase reaching a peak at $\sigma \sim 0.55$. For calculations **A**, the mismatch between numerical and experimental torque in this point is of $\sim 3.5\%$. Using strategy **B**, this discrepancy is reduced to $\sim 1.5\%$, due to the introduction of the draft tube in the computational domain. After $\sigma \sim 0.55$, the computed curves decrease more quickly than the experimental one, reaching the minimum for higher σ values.

More reliable comparisons can be obtained applying the **C** strategy, where the total pressure is considered as inlet boundary condition on the computational domain **D2**. This methodology allows to numerically reproduce experimental test conditions and the obtained results are in good quantitative and qualitative agreement with measured data. The maximum discrepancy between numerical and experimental torque is smaller than 1.5% . The numerical torque drop

beginning point is very close to the experimental one (at $\sigma \sim 0.60$). The relative torque reduction is correctly predicted until $\sigma = 0.57$. For smaller *Thoma* numbers, the cavitating flow becomes unstable and the steady approach applied in this work is no longer suitable. Thus, unsteady calculations should be carried out to improve the predictions and to analyze cavitating flows corresponding to the smallest σ values. Figure 3 (b) presents experimental and computed non-dimensional σ -*break* curves evolutions. All of the numerical results seem to be in good agreement with the experiments, but the analysis of the efficiency drop curves is biased by cross-variations in H , Q , and T .

4.3. Cavitating flow analyses

The numerical methodology **C** has been validated comparing numerical and experimental cavities for two points of the computed σ -*break* curve, $\sigma = 0.60$ and 0.57 .

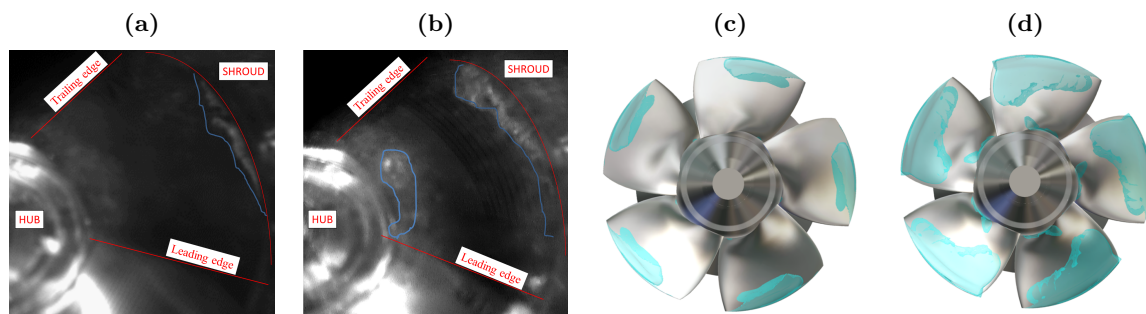


Figure 4. Frontal view of : Experimental observations at $\sigma = 0.60$ (a) and at $\sigma = 0.48$ (b); Computed iso-surfaces of density ($\rho = 980\text{kg/m}^3$) at $\sigma = 0.60$ (c) and at $\sigma = 0.57$ (d).

Experimentally, two vapor structures have been observed in the flow:

- (i) An attached cavitation sheet appears near the shroud at $\sigma = 0.60$ (figure 4 (a)). It increases from the leading edge to the trailing edge, covering the whole tip extension at $\sigma = 0.48$ (figure 4 (b));
- (ii) A vapor structure starts from the leading edge near the runner hub, extending along the blade root in the opposite direction to the runner rotation at $\sigma = 0.48$ (figure 4 (b)).

The cavitation behavior obtained by numerical simulations are reported in figure 4 (c) and in figure 4 (d), respectively and they are in a good qualitative agreement with experimental visualizations. The cavities situated on the blade tip and near the hub are well-predicted at $\sigma = 0.60$, and extend along the profile to the trailing edge at $\sigma = 0.57$.

4.4. Blade loading analyses

The static pressure distributions around the blade for different σ values have been analyzed to investigate the influence of the cavitation on the pressure fields and, consequently, on the torque.

Figure 5 shows the different sections considered for the study of the pressure profiles: a section near the hub (1% of the blade height), the mid-span plane (50% of the blade height) and a section near the shroud (95% of the blade height). The blade loads at different planes are drawn in figure 6 in non-cavitating regime (blue line with the diamonds), at $\sigma = 0.60$ (black dashed line with squares) and at $\sigma = 0.57$ (red line with the circles). The static pressure has been plotted using the normalized pressure coefficient, C_P , defined in equation 7

$$C_P = \frac{P - P_V}{\frac{1}{2}\rho(\omega R)^2}, \quad (7)$$

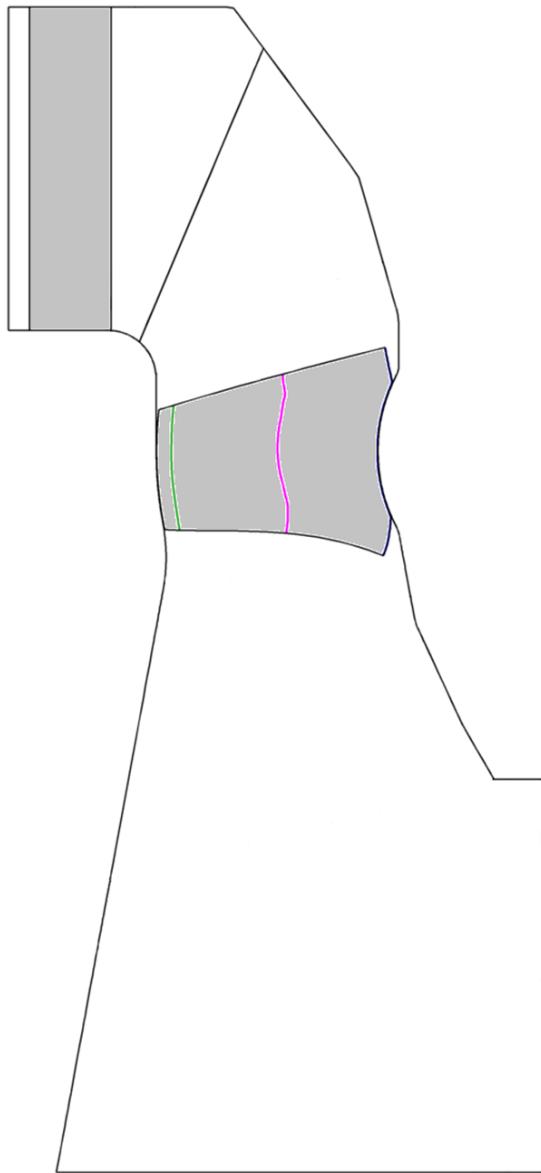


Figure 5. Blade sections at 1%(blue line), 50%(pink line) and 95%(green line) represented in the meridian view considered for the pressure profiles analysis.

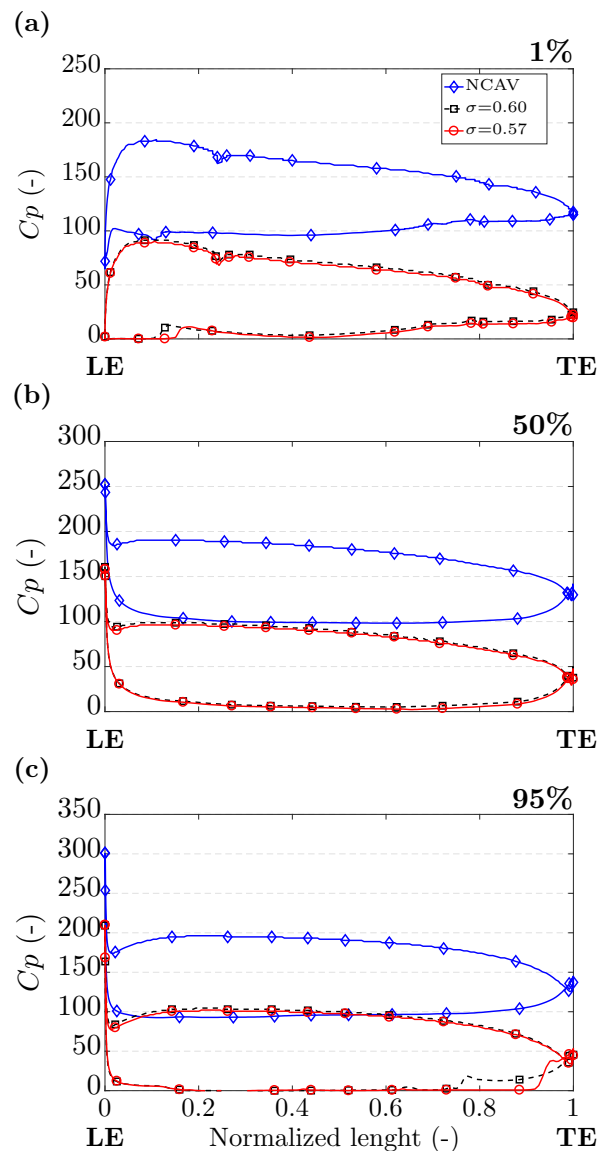


Figure 6. Pressure distribution around the blade for decreasing σ values at (a) near the hub (1%), (b) mid-span (50%) and (c) near the shroud (95%). LE=leading edge; TE=trailing edge.

where R is the radius of the runner. According to numerical results for considered *Thoma* numbers, the presence of the cavitation in the runner does not influence the blade loading at mid-span. Close to the shroud, the loading is slightly modified at the blade leading edge. The cavitation influence is more perceptible at the trailing edge, leading to a decrease of the runner work in this region. These analyses agree well with flow visualizations shown in figures 4. Perturbations of the leading edge pressure distribution can be observed also near the hub. The load reduction is observed when the cavitation appears on the blade root, close to the leading edge of the blade suction side (figures 4 (c)–(d)). These progressive alterations of the blade loading on the hub and near the shroud leads to a gradual decrease of the machine torque, T ,

(figure 3 (a)), in comparison to the non-cavitating case. Modification of the pressure loading on the blade pressure side is not observed with the σ reduction.

5. Conclusions

The aim of the present work was to develop a numerical methodology to predict the cavitation phenomena occurring in a Kaplan turbine and their influence on the machine performances. Three-dimensional *RANS* equations were solved on two computational domains testing different sets of boundary conditions. Cavitation was included in simulations by a homogeneous approach coupled with a barotropic state law. According to numerical results obtained and based on comparisons with available experimental data, a reliable computational strategy was finally proposed.

The first step of the methodology was to ensure a correct numerical reproduction of the turbine operating point in non-cavitating conditions, targeting the measured torque value. An iterative procedure was carried out on a simplified computational domain (including a single periodic interblades guide vane/runner/cone channel) to find the inlet mass flow rate value allowing to reduce the mismatch between experimental and numerical torque. Afterwards, the draft tube was included in the domain and cavitating simulations were performed comparing two inlet conditions: the discharge and the total pressure. The change of inlet boundary condition led to improve the methodology, maintaining a constant head along the σ -break curve, as during experimental tests. The results obtained considering the torque evolution, the σ -break curve and the vapor structures development appeared in a well-agreement with experimental data. At smallest values of the σ , the cavitating flows become unstable, and the steady approach presented in this article is no longer adequate. Unsteady simulations are in progress to improve the prediction and the analyses of more developed cavitating regimes.

Acknowledgments

The present work was funded by a French *FUI* grant. The authors acknowledge *GE Renewable Energy* (Grenoble, France) for providing experimental data and technical support. Authors would also to thank Rémi Lestriez of *Numibérica* for his huge contribution to this work.

References

- [1] Delannoy Y and Kueny J L 1990 *ASME Cavitation Multi-Phase Flow Forum* **109** 153–159
- [2] Singhal A, Vaidya N and Leonard A 1997 *Proc. of the ASME/FEDSM Conf.* **1** 97–3272
- [3] Zwart P, Gerber A and Belamri T 2004 *Proc. of 5th Int. Conf. on Multiphase Flow* **1** 1–11
- [4] Balint D, Resiga R, Muntean S and Anton I 2006 *Proc. of the 13th Int. Conf. on Fluid Flow Technologies* **1** 980–986
- [5] Leguizamón S, Ségoufin C, Hai-Trieu P and Avellan F 2017 *J. Fluids Eng.* **139** 8. 061301
- [6] Jošt D, Morgut M, Škerlavaj A and Nobile E 2015 *Proc. 6th IAHR Int. Meeting of the WG on Cavitation and Dynamic Problems in Hydraulic Machinery and Systems* **1** 43–50
- [7] Ishii M and Hibiki T 2011 *Thermo-Fluid Dynamics of Two-Phase Flow* (New York: Springer-Verlag)
- [8] Coutier-Delgosha O, Fortes-Patella R, Reboud J L, Stoffel B and Hofmann M 2003 *J. Fluids Eng.* **125** 970–978
- [9] Pouffary B, Fortes-Patella R, Reboud J L and Lambert P A 2008 *J. Fluids Eng.* **130** 061301
- [10] Ješe U, Fortes-Patella R and Antheaume S 2014 *IOP Conf. Ser.: Earth Environ. Sci.* **22** 032048
- [11] Reboud J L, Stutz B and Coutier-Delgosha O 1998 *Proc. Second Intl Symp. on Cavitation* **1** 203–208
- [12] Goncalves E and Fortes-Patella R 2009 *Computers & Fluids* **38** 1682–96
- [13] Menter F, Kuntz M and Langtry R 2003 *Proc. of the 4th Int. Symp. on Turbulence, Heat and Mass Transfer* **1** 625–632